

# RF-GPT: Teaching AI to See the Wireless World

Hang Zou, Yu Tian, Bohao Wang, Lina Bariah, Samson Lasaulce, Chongwen Huang, and Mérouane Debbah

**Abstract**—Large language models (LLMs) and multimodal models have become powerful general-purpose reasoning systems. However, radio-frequency (RF) signals, which underpin wireless systems, are still not natively supported by these models. Existing LLM-based approaches for telecom focus mainly on text and structured data, while conventional RF deep-learning models are built separately for specific signal-processing tasks, highlighting a clear gap between RF perception and high-level reasoning. To bridge this gap, we introduce RF-GPT, a *radio-frequency language model* (RFLM) that utilizes the visual encoders of multimodal LLMs to process and understand RF spectrograms. In this framework, complex in-phase/quadrature (IQ) waveforms are mapped to time-frequency spectrograms and then passed to pretrained visual encoders. The resulting representations are injected as RF tokens into a decoder-only LLM, which generates RF-grounded answers, explanations, and structured outputs. To train RF-GPT, we perform supervised instruction fine-tuning of a pretrained multimodal LLM using a fully synthetic RF corpus. Standards-compliant waveform generators produce wideband scenes for six wireless technologies, from which we derive time-frequency spectrograms, exact configuration metadata, and dense captions. A text-only LLM then converts these captions into RF-grounded instruction–answer pairs, yielding roughly 12,000 RF scenes and 0.625 million instruction examples without any manual labeling. Across benchmarks for wideband modulation classification, overlap analysis, wireless-technology recognition, WLAN user counting, and 5G NR information extraction, RF-GPT achieves strong multi-task performance, whereas general-purpose VLMs with no RF grounding largely fail.

**Index Terms**—Radio frequency language models, vision-language models, radio frequency signals, modulation classification, spectrograms, RF-GPT

## I. INTRODUCTION

Large language models (LLMs) have significantly advanced natural language processing, enabling powerful capabilities in long-form generation, code synthesis, tool use, and multi-step reasoning. Multimodal systems now extend these capabilities beyond text, where multimodal and vision–language models (VLMs), such as GPT-4o [1], Gemini [2], LLaVA [3], Qwen-VL [4], and InternVL [5] integrate image and text inputs to support visual reasoning, captioning, and visual question answering, among other tasks. On the other hand, in the audio domain, large transformer-based models such as Whisper [6], Qwen2-Audio [7], Minimax-Speech [8] demonstrate that massive unlabeled speech and sound corpora can be leveraged to learn robust representations for transcription, generation, and

H. Zou, Y. Tian, B. Wang, L. Bariah and M. Debbah are with Research Institute for Digital Future, Khalifa University, 127788 Abu Dhabi, UAE (e-mails: {hang.zou, yu.tian, lina.bariah, merouane.debbah}@ku.ac.ae).

B. Wang and C. Huang are with College of Information Science and Electronic Engineering, Zhejiang University, 310027, Hangzhou, China (email: {bohao.wang, chongwen.huang}@zju.edu.cn)

S. Lasaulce is with Université de Lorraine, CNRS, CRAN, F-54000 Nancy, France (email: samson.lasaulce@univ-lorraine.fr).

audio understanding. Despite these advances in text, vision, and audio, radio-frequency (RF) signals, which represent the physical layer for wireless communications, radar sensing, and integrated sensing-and-communications (ISAC), have not yet been integrated into these foundation model frameworks.

Existing machine learning-driven RF intelligence is mainly designed based on narrow, task-specific models, for automatic modulation classification, channel estimation, beam selection, interference identification, and spectrum sensing [9], to name a few. These models are typically trained on small, heterogeneous datasets under constrained assumptions about channel models, hardware impairments, and traffic patterns, and they are evaluated on task-specific metrics. While such models can achieve high accuracy, they exhibit several limitations. First, each task requires its own architecture, dataset, and training pipeline, resulting in limited reuse across tasks. Second, building diverse and well-labeled RF datasets is expensive and usually requires expert annotation, making large-scale supervision difficult. Third, models trained under particular setups experience degraded performance when deployed under different SNR ranges, channel conditions, or hardware scenarios. Finally, most RF models produce only labels or regression outputs, without explanations or a natural interface for human interaction. Within this context, a language-model-based approach introduces a radical change in these approaches in two important ways. First, it allows multiple RF tasks to be achieved within a single model through instructions, rather than through separate architectures. Second, it introduces an interface for reasoning and interaction, where the model can describe what it observes, justify its predictions, and respond to follow-up questions. Instead of training a new neural network for each RF objective, tasks can be designed as prompts that are executed over a shared representation.

Despite recent progress on wireless and RF foundation models, such as WFM [10], LWM [11], and WirelessGPT-like channel models [12], most existing approaches still rely on task-specific output heads or per-task fine-tuning to achieve competitive performance on various downstream tasks. In practice, each new application (e.g., channel estimation, localization, sensing, or RF classification) requires its own prediction head, loss design, and fine-tuning pipeline on labeled data, significantly limiting the potential of an RF *foundation model*. At the same time, many of these models are relatively small and optimized for a small set of benchmarks, making it difficult to balance performance across heterogeneous tasks or to scale them according to the famous scaling law [13].

In parallel, the 6G research roadmap envisions AI-native networks that integrate sensing, communication, computing, and control, with autonomous, intent-driven operation across the radio access and core network [14]–[16]. Within this vision, LLMs have been proposed as unified interfaces for

knowledge access, reasoning, tool orchestration, and policy optimization, enabling automated fault diagnosis, configuration generation, and closed-loop network management. Early work on *LLM4Telecom* has explored network and service management assistants, domain-specialized instruction-tuned models, and agentic workflows that connect LLMs to monitoring systems, operations support systems (OSS) and business support systems (BSS) data [17]–[21]. Telecom-specific LLMs, such as *TelecomGPT* [22], integrate domain knowledge directly into the language model to improve its reasoning capabilities over alarms, KPIs, logs, and configuration data.

However, it is important to emphasize that the integration of LLMs into telecom networks is largely *text-centric*. Existing Telecom LLMs are primarily designed to process human-readable data, including tickets, log messages, configuration tables, and structured KPIs. They do not directly process observations pertinent to the physical layer, such as RF waveforms, spectrograms, or channel estimates. Subsequently, this modality gap prevents the use of LLMs in advanced RF-based tasks that require direct access to the RF spectrum, such as identifying coexisting technologies, detecting interference, analyzing occupancy patterns, or validating standard compliance at the signal level. Having said that, future AI-native networks are not envisaged to support reasoning over text and structured data only, but will require as well deep RF perception capabilities that are explainable, queryable, and integrated with higher-level decision making.

These limitations motivate the development of *radio-frequency language models* (RFLMs), which are foundation models that can process RF data and respond in natural language. In principle, an RFLM is a conditional language model grounded on RF tokens. Given an RF recording, it should be able to answer questions such as “Which modulations and technologies are present in this band?”, “Are there overlapping transmissions and what is their time–frequency relationship?”, or “Is this behavior compliant with the relevant wireless standard?”. Beyond simple classification, an RFLM can provide textual explanations, structured JSON summaries for downstream controllers, and interactive dialogue with RF engineers or higher-level LLM agents. This language interface is aimed for practical reasons, including providing a unified instruction-following interface that comprises a wide range of RF downstream tasks, facilitating the integration of domain knowledge (e.g., ITU/3GPP standards, link-budget formulas, antenna constraints) and human feedback, as well as allowing human operators and autonomous agents to query, inspect, and manage RF behavior using plain language. In this sense, RF modeling becomes more flexible and interactive, rather than isolated predictors.

RF systems inherently generate large amounts of data (wideband monitoring, SDR deployments, cellular logs), and realistic simulators can produce vast amounts of labeled or semi-labeled signals under controlled conditions. This makes RF a promising candidate for self-supervised and synthetic pretraining. Using realistic waveform generators, we can generate signal-metadata samples, with accurate ground truth, such as modulation type, SNR, bandwidth, or resource allocation. Such a pipeline reduces the reliance on expert annotations

and enables large-scale pretraining and instruction tuning. A pretrained RFLM can then be compressed or adapted for deployment across different RF scenarios, and can serve as an RF reasoning module across O-RAN, non-terrestrial networks, and ISAC scenarios, among other scenarios.

However, it is worth emphasizing that realizing such an RFLM is challenging. Unlike images and audio signals, RF waveforms are time-series, complex-valued signals sampled at very high rates, and understanding them depends on understanding time–frequency structure, protocol standards, and propagation effects. To the best of the authors’ knowledge, large-scale datasets of real RF signals in diverse environment with expert textual annotations do not exist in the literature. Building such a dataset requires long-term RF measurements, specialized hardware, and domain experts for labeling. Over-the-air data collection also raises privacy concerns, and typical RF environments are highly imbalanced, with rare but critical scenarios, such as extreme interference or unusual coexistence, being difficult to capture.

In this paper, we propose **RF-GPT**, a radio-frequency language model that integrates RF spectrograms into a multimodal LLM. To achieve our objectives, we treat RF spectrograms as visual inputs and reuse the visual components of advanced vision–language models. Specifically, we first convert complex in-phase/quadrature (IQ) samples into time–frequency spectrograms using STFT. These spectrograms are mapped to pseudo-RGB or grayscale images and encoded by a pretrained vision encoder to produce RF tokens. The tokens are then projected into the language-model embedding space through a lightweight adapter, after which a decoder-only LLM generates RF-grounded text conditioned on this RF prefix. To overcome the lack of RF–text pairs, we build a large synthetic spectrogram–caption dataset using realistic waveform generators for wireless technologies, record full configuration metadata, convert it into technical captions using a deterministic captioning pipeline, and then use a strong text-only LLM to synthesize diverse instruction–answer pairs (descriptions, counting, overlap analysis, structured JSON). We then perform RF-grounded supervised fine-tuning on multimodal LLM backbones (e.g., Qwen2.5-VL [4]) on this synthetic RF instruction set, without any human-annotated spectrogram labels. At inference time, RF-GPT takes an RF waveform/spectrogram and a natural-language query and returns explanations, predictions, or structured outputs that reflect RF-aware reasoning. We evaluate the model on a benchmark suite covering wideband modulation classification, overlap analysis, wireless-technology recognition, WLAN user counting, and 5G NR information extraction. The main contributions of this paper are summarized as follows:

- We formulate the notion of a radio-frequency language model (RFLM) as a conditional language model grounded on RF tokens, and realize this concept through **RF-GPT**, which integrates RF spectrograms into a multimodal LLM via a vision encoder and a lightweight modality adapter through simple linear projection.
- We design standards-compliant pipelines to synthesize a large RF spectrogram corpus for wideband settings and six wireless technologies, including 5G NR, LTE,

UMTS, WLAN, DVB-S2, and Bluetooth, and introduce deterministic captioning schemes that convert signal-level attributes into structured textual descriptions.

- We propose an automatic instruction-synthesis framework that converts RF captions into a diverse set of RF-grounded instruction–answer pairs, including explanation-style questions, quantitative queries (e.g., counts, overlaps), and structured JSON outputs, and we construct benchmarks that evaluate component recognition, overlap reasoning, technology identification, user counting, and NR-specific attribute extraction.
- We fine-tune pretrained multimodal LLMs on these synthetic RF instructions to obtain RF-GPT and demonstrate that RF grounding enables them to perform a range of RF understanding tasks on RF signals, including modulation classification, technology recognition, overlap analysis, and free-form RF question answering, while generic VLMs without RF grounding fail on the same benchmarks.

## II. PROBLEM FORMULATION AND RF-GPT ARCHITECTURE

In this section, we present the RF-GPT architecture adopted in this work. Let  $\mathbf{x} \in \mathbb{C}^T$  denotes a complex baseband IQ sequence of length  $T$  samples, and let  $\mathbf{y} = (y_1, \dots, y_N)$  denote a text sequence of  $N$  tokens from a vocabulary  $\mathcal{V}$ . This text sequence is generally relevant to the RF signals, e.g., a description of their characteristics or intents associated with them. We denote by  $\phi_{\text{RF}}$  an RF encoder that maps the raw IQ sequence into a sequence of  $M$  RF tokens in a latent space,

$$\phi_{\text{RF}} : \mathbb{C}^T \rightarrow \mathbb{R}^{M \times d}, \quad (1)$$

where  $d$  is the embedding dimension of each RF token. In our formulation, an RFLM is a conditional language model that generates a token sequence  $\mathbf{y}$  given an RF input  $\mathbf{x}$  that has been encoded into a sequence of RF tokens  $\phi_{\text{RF}}(\mathbf{x})$ . The model defines the autoregressive conditional distribution as

$$\mathcal{P}_{\Theta}(\mathbf{y} | \phi_{\text{RF}}(\mathbf{x})) = \prod_{t=1}^N \mathcal{P}_{\Theta}(y_t | \mathbf{y}_{<t}, \phi_{\text{RF}}(\mathbf{x})), \quad (2)$$

where  $\mathbf{y}_{<t} = (y_1, \dots, y_{t-1})$  and  $\Theta$  collects all trainable parameters of RF-GPT. The RF tokens serve as a prefix that conditions an autoregressive language model on the RF input.

The basic structure of RF-GPT is illustrated in Fig. 1. RF-GPT consists of (i) a Transformer-based RF encoder, (ii) an RF adapter (linear projection) that projects RF tokens into the language-model embedding space, and (iii) a decoder-only LLM that produces RF-grounded text outputs. In the following, we describe each component and the RF-grounded supervised fine-tuning (SFT) procedure.

### A. RF Encoding via Spectrograms and Vision Encoder

Applying Transformers directly to raw IQ sequences sampled at RF rates is computationally infeasible [23] and ignores the strong inductive bias of time–frequency structure [9]. Hence, we first map an RF signal  $\mathbf{x}$  to a two-dimensional time–frequency representation using a short-time

Fourier transform (STFT). Let the sampling rate be denoted by  $f_s$ , and let  $x[n]$  represents the  $n$ -th complex sample at time  $t = n/f_s$ . We compute the STFT with window  $w[n]$ , fast Fourier transform (FFT) size  $F$ , and hop size  $H_{\text{hop}}$ ,

$$S[k, t] = \sum_n x[n] w[n - tH_{\text{hop}}] e^{-j \frac{2\pi}{F} kn}, k \in [0, F-1], \quad (3)$$

where  $t$  represents the time index and  $S[k, t] \in \mathbb{C}$  is the complex STFT coefficient at frequency bin  $k$  and frame  $t$ . We then convert the complex spectrogram to a magnitude (or power) spectrogram in dB by applying log compression, as follows

$$A_{\text{dB}}[k, t] = 10 \log_{10}(|S[k, t]|^2 + \varepsilon), \quad (4)$$

where  $\varepsilon > 0$  is a small constant for numerical stability. The resulting time–frequency matrix is normalized and mapped to an image  $\mathbf{I} \in \mathbb{R}^{H \times W \times C}$ , where  $H$  and  $W$  are the image height and width and  $C$  is the number of channels. We either consider  $A_{\text{dB}}$  as a single-channel grayscale image ( $C = 1$ ) or apply a fixed colormap (e.g., viridis) to obtain a pseudo-RGB image ( $C = 3$ ). This yields an RF spectrogram image that can be processed by a standard vision encoder  $\mathcal{E}_{\text{v}}$ . We define the complete RF encoder  $\phi_{\text{RF}}$  as the composition of the spectrogram pipeline and the vision pipeline, as

$$\phi_{\text{RF}}(\mathbf{x}) = \mathcal{E}_{\text{v}}(\mathbf{I}) = \mathcal{E}_{\text{v}}(\text{Spec}(\mathbf{x})), \quad (5)$$

where  $\text{Spec}(\cdot)$  denotes the spectrogram pipeline (STFT + magnitude/dB + colormap).

**Patch embedding.** The spectrogram image  $\mathbf{I}$  is partitioned into a regular grid of non-overlapping patches of size  $P \times P$  pixels, where both  $H$  and  $W$  are divisible by  $P$ . The number of patches (and thus RF tokens) is  $M = \frac{H}{P} \cdot \frac{W}{P}$ . Let  $\mathbf{x}_i \in \mathbb{R}^{P^2 C}$  denote the vector obtained by flattening the  $i$ -th patch (row-major order), for  $i = 1, \dots, M$ . Each patch is linearly projected to a  $d$ -dimensional embedding using a learnable matrix  $\mathbf{E} \in \mathbb{R}^{d \times (P^2 C)}$ ,

$$\mathbf{e}_i = \mathbf{E} \mathbf{x}_i \in \mathbb{R}^d, \quad i = 1, \dots, M. \quad (6)$$

This patchification and linear projection step acts as an RF tokenizer, turning each spectrogram into a sequence of  $M$  RF tokens that the language model can consume. We also use a learnable positional embedding  $\mathbf{p}_i \in \mathbb{R}^d$  for each patch index  $i$ , which encodes its 2D location on the spectrogram grid (time–frequency position). The input token sequence to the transformer encoder is then given by

$$\mathbf{z}_i^{(0)} = \mathbf{e}_i + \mathbf{p}_i, \quad i = 1, \dots, M, \quad (7)$$

and we stack them into

$$\mathbf{Z}^{(0)} = \begin{bmatrix} (\mathbf{z}_1^{(0)})^\top \\ \vdots \\ (\mathbf{z}_M^{(0)})^\top \end{bmatrix} \in \mathbb{R}^{M \times d}. \quad (8)$$

Unlike some ViT variants [24], [25], we do not prepend a special classification token, instead, all  $M$  patch tokens are treated as RF tokens and later passed to the language model.

**Transformer encoder layers.** The matrix  $\mathbf{Z}^{(0)}$  is processed by  $L$  stacked transformer encoder blocks. Each block consists

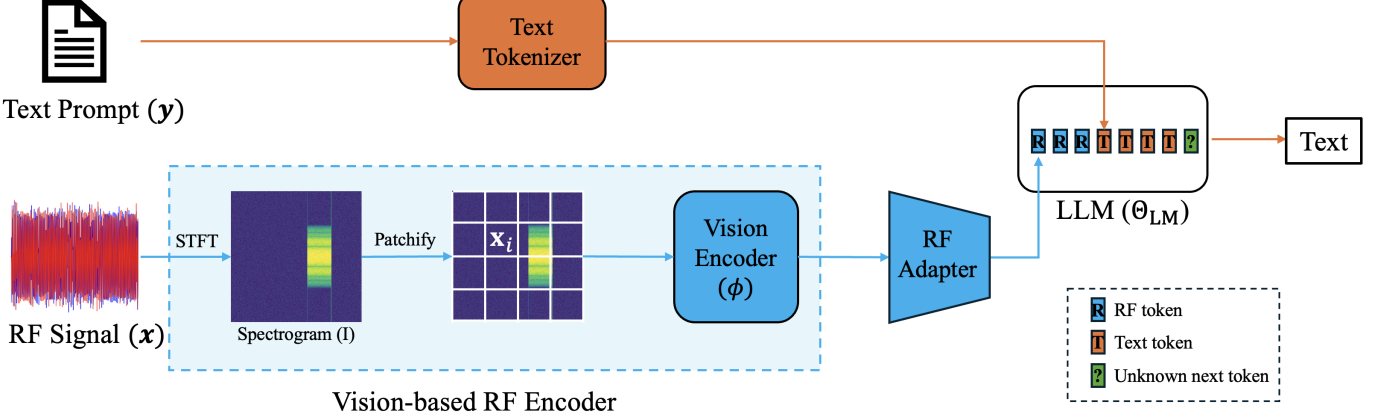


Fig. 1: Basic structure of RF-GPT, comprising a visio-based radio-frequency (RF) encoder (implemented by a vision encoder on RF spectrograms), an RF adapter (linear projection) that projects RF embeddings to the LLM dimension, and a decoder-only LLM. STFT stands for short-time Fourier transform.

of multi-head self-attention (MHA) followed by a position-wise multi-layer perceptron (MLP), both wrapped with residual connections and layer normalization. Given  $\mathbf{Z}^{(\ell)} \in \mathbb{R}^{M \times d}$  as the input to layer  $\ell$  ( $\ell = 0, \dots, L - 1$ ), the output  $\mathbf{Z}^{(\ell+1)}$  is obtained as

$$\widetilde{\mathbf{Z}}^{(\ell)} = \mathbf{Z}^{(\ell)} + \text{MHA}(\text{LN}(\mathbf{Z}^{(\ell)})), \quad (9)$$

$$\mathbf{Z}^{(\ell+1)} = \widetilde{\mathbf{Z}}^{(\ell)} + \text{MLP}(\text{LN}(\widetilde{\mathbf{Z}}^{(\ell)})), \quad (10)$$

where  $\text{LN}(\cdot)$  is layer normalization and the MLP is a two-layer feed-forward network (FFN) with nonlinearity, applied row-wise as

$$\text{MLP}(\mathbf{z}) = \sigma(\mathbf{z}\mathbf{W}_1 + \mathbf{b}_1)\mathbf{W}_2 + \mathbf{b}_2, \quad (11)$$

for learnable weights  $\mathbf{W}_1, \mathbf{W}_2$  and biases  $\mathbf{b}_1, \mathbf{b}_2$ , and activation function  $\sigma(\cdot)$  (e.g., GELU).

The multi-head self-attention (MHA) operates as follows. For a given input  $\mathbf{U} \in \mathbb{R}^{M \times d}$ , the  $h$ -th attention head computes

$$\mathbf{Q}_h = \mathbf{U}\mathbf{W}_h^Q, \quad \mathbf{K}_h = \mathbf{U}\mathbf{W}_h^K, \quad \mathbf{V}_h = \mathbf{U}\mathbf{W}_h^V, \quad (12)$$

$$\mathbf{A}_h = \text{softmax}\left(\frac{\mathbf{Q}_h \mathbf{K}_h^\top}{\sqrt{d_k}}\right), \quad \mathbf{H}_h = \mathbf{A}_h \mathbf{V}_h, \quad (13)$$

where  $\mathbf{W}_h^Q, \mathbf{W}_h^K, \mathbf{W}_h^V \in \mathbb{R}^{d \times d_k}$  are learnable projection matrices (query, key, and value for head  $h$ ),  $d_k$  is the head dimension, and softmax is applied row-wise over the attention scores. The outputs of all heads are concatenated and linearly projected, as follows

$$\text{MHA}(\mathbf{U}) = [\mathbf{H}_1 \parallel \mathbf{H}_2 \parallel \dots \parallel \mathbf{H}_H] \mathbf{W}^O, \quad (14)$$

where  $\mathbf{W}^O \in \mathbb{R}^{(Hd_k) \times d}$  is the projection matrix and  $H$  represents the number of attention heads. After  $L$  layers, the final patch embeddings are represented as

$$\mathbf{h}_i = \mathbf{z}_i^{(L)} \in \mathbb{R}^d, \quad i = 1, \dots, M. \quad (15)$$

These vectors form the RF-grounded latent sequence  $h_{1:M}$  used for downstream conditioning.

**Remark.** In our framework, the vision encoder *serves as the RF encoder* by treating the spectrogram as an image and encoding time–frequency patterns such as modulation structure, resource allocation, interference, and coexistence into a sequence of latent RF tokens. There are two main motivations for transforming a vision encoder into an RF encoder, namely, (i) RF signals span very different carrier frequencies, bandwidths, and sampling rates across technologies, making it difficult to design a single raw-IQ tokenizer that is simultaneously efficient and robust for narrowband, wideband, and multi-standard scenarios, and (ii) the STFT serves as an effective RF feature extractor, while a vision encoder pretrained on large-scale image datasets can extract universal semantic structure from images, including spectrograms.

A key design decision in RF-GPT is to operate on magnitude spectrograms rather than raw IQ signals. From a time-frequency analysis viewpoint, the spectrogram is a smoothed energy distribution associated with the signal, and can be seen as a windowed version of Wigner–Ville type representations [26]. As such, many RF attributes of interest, e.g., occupied bandwidth, center frequency and Doppler shifts, burst timing, time-frequency sparsity patterns, and even modulation structure, are encoded geometrically in the spectrogram and are therefore accessible to a vision encoder.

It is important to distinguish between two regimes. First, *true phase retrieval* aims to reconstruct the entire complex baseband waveform from magnitude-only measurements (e.g., STFT magnitude). This problem is nontrivial, but the phase-retrieval literature shows that, under suitable redundancy and support assumptions, a signal can be uniquely determined (up to a global phase) and stably recovered from such magnitude data; see, e.g., work on STFT phase retrieval [27] and convex formulations such as PhaseLift [28]. Second, in our setting we do not attempt to reconstruct  $x[n]$  itself, but only to infer task-relevant attributes such as modulation family, technology, SNR regime, or overlap structure. These tasks are many-to-one mappings of the waveform and depend primarily on the time-frequency energy patterns, not on the exact sample-wise phase.

RF-GPT therefore uses magnitude-only spectrograms as a rich but lossy front-end representation. While they are not sufficient for all possible RF tasks (e.g., those requiring absolute phase information or precise multi-antenna phase relationships), they retain enough structure to support the perception-oriented tasks considered in this work. In Sec. IV we empirically validate that this spectrogram-based approach allows the model to recover the RF attributes required by our benchmarks with high accuracy. With the RF encoding pipeline established, we now describe how the resulting RF tokens are used to condition the language model and ground its predictions in RF information.

### B. Language Model Architecture and RF Conditioning

The backbone of RF-GPT is a decoder-only Transformer language model with parameters  $\Theta_{\text{LM}}$ , which are part of the overall parameter set  $\Theta$ . The LLM operates on a sequence of token embeddings  $\mathbf{u}_{1:(M+N)} \in \mathbb{R}^{(M+N) \times d_{\text{LM}}}$ , where  $d_{\text{LM}}$  is the model dimension of the LLM. We add standard positional embeddings e.g., rotary position embeddings (RoPE [29]) to  $\mathbf{u}_{1:(M+N)}$  before passing them to the decoder layers.

First, the RF encoder produces  $M$  visual tokens  $\mathbf{h}_{1:M} = \mathcal{E}_v(I)$ , with  $\mathbf{h}_i \in \mathbb{R}^d$  as defined in the previous subsection. An RF adapter through simple linear projection maps these to the LLM dimension,

$$\mathbf{r}_i = \mathbf{W}_{\text{proj}} \mathbf{h}_i + \mathbf{b}_{\text{proj}} \in \mathbb{R}^{d_{\text{LM}}}, \quad i = 1, \dots, M, \quad (16)$$

where  $\mathbf{W}_{\text{proj}} \in \mathbb{R}^{d_{\text{LM}} \times d}$  and  $\mathbf{b}_{\text{proj}} \in \mathbb{R}^{d_{\text{LM}}}$  are trainable parameters. This linear layer plays the role of a visual-language adapter, similar to the projection modules used in LLaVA-style models [3], mapping the vision-encoder features (which encodes RF information) into the LLM embedding space.

Text tokens  $y_t$  are embedded via a standard lookup table  $\mathbf{E}_{\text{tok}} \in \mathbb{R}^{|\mathcal{V}| \times d_{\text{LM}}}$ :

$$\mathbf{e}_t = \mathbf{E}_{\text{tok}}[y_t] \in \mathbb{R}^{d_{\text{LM}}}, \quad t = 1, \dots, N, \quad (17)$$

with  $|\mathcal{V}|$  the vocabulary size of the LLM backbone. We then form a single joint sequence by concatenating RF and text embeddings:

$$\mathbf{u}_{1:(M+N)} = [\mathbf{r}_1, \dots, \mathbf{r}_M, \mathbf{e}_1, \dots, \mathbf{e}_N]. \quad (18)$$

Let  $\mathbf{U}^{(0)} \in \mathbb{R}^{(M+N) \times d_{\text{LM}}}$  be the matrix whose rows are  $\mathbf{u}_1, \dots, \mathbf{u}_{M+N}$ . The sequence is processed by  $L_{\text{LM}}$  stacked decoder layers. Each layer follows a modern *pre-normalized* Transformer design with root mean square (RMS) normalization, grouped-query attention (GQA) with a causal mask, and a gated Up/Down MLP, as adopted in recent Qwen-series LLMs. For layer  $\ell = 0, \dots, L_{\text{LM}} - 1$  we write

$$\tilde{\mathbf{U}}^{(\ell)} = \mathbf{U}^{(\ell)} + \text{GQA}_{\text{causal}}(\text{RMSNorm}(\mathbf{U}^{(\ell)})), \quad (19)$$

$$\mathbf{U}^{(\ell+1)} = \tilde{\mathbf{U}}^{(\ell)} + \text{MLP}_{\text{gated}}(\text{RMSNorm}(\tilde{\mathbf{U}}^{(\ell)})), \quad (20)$$

where  $\text{RMSNorm}(\cdot)$  is root-mean-square layer normalization [30],  $\text{GQA}_{\text{causal}}$  is grouped-query self-attention [31] with a causal mask, and  $\text{MLP}_{\text{gated}}$  is a gated feed-forward block (Up/Down MLP) [32]. Since decoder-only transformers and these building blocks are not yet standard in RF modeling, we briefly recall their definitions.

**RMS normalization.** For a token vector  $\mathbf{x} \in \mathbb{R}^{d_{\text{LM}}}$ ,  $\text{RMSNorm}$  is defined as

$$\text{RMSNorm}(\mathbf{x}) = \gamma \odot \frac{\mathbf{x}}{\sqrt{\frac{1}{d_{\text{LM}}} \|\mathbf{x}\|_2^2 + \varepsilon}}, \quad (21)$$

where  $\gamma \in \mathbb{R}^{d_{\text{LM}}}$  is a learned scale,  $\varepsilon > 0$  is a small constant, and  $\odot$  denotes element-wise multiplication.  $\text{RMSNorm}$  stabilizes activations while being slightly simpler than standard LayerNorm.

**Grouped-query Attention (GQA).** Let  $\mathbf{U} \in \mathbb{R}^{(M+N) \times d_{\text{LM}}}$  denote a generic layer input. Grouped-query attention uses  $H_q$  query heads and  $H_k$  key-value heads with  $H_q \geq H_k$ . We first compute

$$\mathbf{Q} = \mathbf{U} \mathbf{W}^Q, \quad \mathbf{K} = \mathbf{U} \mathbf{W}^K, \quad \mathbf{V} = \mathbf{U} \mathbf{W}^V, \quad (22)$$

where  $\mathbf{W}^Q \in \mathbb{R}^{d_{\text{LM}} \times H_q d_k}$  and  $\mathbf{W}^K, \mathbf{W}^V \in \mathbb{R}^{d_{\text{LM}} \times (H_k d_k)}$  are learnable projection matrices, and  $d_k$  is the head dimension. To facilitate grouped-query computation, we reshape  $\mathbf{Q}$  into  $H_q$  separate heads and  $\mathbf{K}, \mathbf{V}$  into  $H_k$  groups. Formally, let  $\mathbf{Q}_h \in \mathbb{R}^{(M+N) \times d_k}$  denote the  $h$ -th query head for  $h \in \{1, \dots, H_q\}$ , and let  $\mathbf{K}_{g(h)}, \mathbf{V}_{g(h)} \in \mathbb{R}^{(M+N) \times d_k}$  represent the key and value heads shared by the group associated with query head  $h$ . The grouping is determined by the index function  $g(h) = \lfloor (h-1)/r \rfloor + 1$ , where  $r = H_q/H_k$  is the group size, mapping the  $h$ -th query head to its corresponding key-value group index. With a causal attention mask  $M_{\text{causal}} \in \mathbb{R}^{(M+N) \times (M+N)}$  (entries 0 for allowed positions and  $-\infty$  otherwise), GQA is

$$\mathbf{A}_h = \text{softmax} \left( \frac{\mathbf{Q}_h \mathbf{K}_{g(h)}^\top}{\sqrt{d_k}} + M_{\text{causal}} \right),$$

$$\mathbf{H}_h = \mathbf{A}_h \mathbf{V}_{g(h)}, \quad (23)$$

and the heads are concatenated and linearly projected back to  $d_{\text{LM}}$ :

$$\text{GQA}_{\text{causal}}(\mathbf{U}) = [\mathbf{H}_1 \parallel \dots \parallel \mathbf{H}_{H_q}] \mathbf{W}^O, \quad (24)$$

with  $\mathbf{W}^O \in \mathbb{R}^{(H_q d_k) \times d_{\text{LM}}}$ . The causal mask enforces that position  $t$  attends only to positions  $\leq t$ , ensuring autoregressive generation.

**Gated Up/Down MLP.** The feed-forward block uses a gated Up/Down structure (often instantiated with a SwiGLU-style activation) instead of a plain two-layer MLP. For an input matrix  $\mathbf{X} \in \mathbb{R}^{T \times d_{\text{LM}}}$ , we compute

$$\mathbf{U}_{\text{up}} = \mathbf{X} \mathbf{W}_{\text{up}} + \mathbf{b}_{\text{up}}, \quad (25)$$

$$\mathbf{U}_{\text{gate}} = \mathbf{X} \mathbf{W}_{\text{gate}} + \mathbf{b}_{\text{gate}}, \quad (26)$$

where  $\mathbf{W}_{\text{up}}, \mathbf{W}_{\text{gate}} \in \mathbb{R}^{d_{\text{LM}} \times d_{\text{ff}}}$  project into a larger hidden dimension  $d_{\text{ff}}$ , and  $\mathbf{b}_{\text{up}}, \mathbf{b}_{\text{gate}} \in \mathbb{R}^{d_{\text{ff}}}$ . A pointwise nonlinear gating (e.g., SwiGLU) is then applied:

$$\mathbf{G} = \phi_{\text{SwiGLU}}(\mathbf{U}_{\text{gate}}) \odot \mathbf{U}_{\text{up}}, \quad (27)$$

$$\text{MLP}_{\text{gated}}(\mathbf{X}) = \mathbf{G} \mathbf{W}_{\text{down}} + \mathbf{b}_{\text{down}}, \quad (28)$$

with  $\mathbf{W}_{\text{down}} \in \mathbb{R}^{d_{\text{ff}} \times d_{\text{LM}}}$  and  $\mathbf{b}_{\text{down}} \in \mathbb{R}^{d_{\text{LM}}}$ . The gating mechanism improves expressivity at similar or lower computational cost than a standard two-layer MLP.

Finally, the last decoder layer produces  $\mathbf{U}^{L_{LM}} \in \mathbb{R}^{(M+N) \times d_{LM}}$ . We take the final  $N$  positions corresponding to the text tokens (indices  $M + 1$  to  $M + N$ ) and apply a linear output head and softmax to obtain the conditional distribution  $\mathcal{P}_\Theta(\mathbf{y} \mid \phi_{RF}(\mathbf{x}))$  in (2). Apart from the RF tokens being concatenated as a prefix, the LLM follows a modern architecture of LLMs with grouped-query attention, RMSNorm, and gated MLPs (e.g., Qwen- and LLaMA-style models).

### C. RF-Grounded Supervised Fine-Tuning

With the model structure of RF-GPT in place, we now discuss how to inject knowledge of RF signals into it. To adapt a generic VLM into an RFLM, we perform RF-grounded supervised fine-tuning (SFT) on a synthetic instruction dataset built from standards-compliant waveform generators. We assume access to a dataset

$$\mathcal{D}_{RF} = \{(\mathbf{x}^{(i)}, \mathbf{q}^{(i)}, \mathbf{y}^{(i)})\}_{i=1}^K, \quad (29)$$

where  $\mathbf{x}^{(i)}$  is an RF waveform (IQ samples) that can be converted into a spectrogram image as described in Sec. II-A,  $\mathbf{q}^{(i)}$  is a natural-language instruction or question about the corresponding spectrogram (e.g., “Describe the signal types and overlaps in this RF scene.”), and  $\mathbf{y}^{(i)}$  is the desired answer (e.g., a caption, explanation, or JSON summary). These triplets are constructed in two stages, namely, RF spectrogram captioning and RF instruction synthesis (see Sec. III). Given this dataset, RF-GPT is trained to minimize the standard autoregressive cross-entropy loss over the answer tokens, conditioned on both the RF tokens and the instruction, as follows

$$\mathcal{L}(\Theta) = - \sum_{(\mathbf{x}, \mathbf{q}, \mathbf{y}) \in \mathcal{D}_{RF}} \sum_{t=1}^{|\mathbf{y}|} \log \mathcal{P}_\Theta(y_t \mid \mathbf{y}_{<t}, \mathbf{q}, \phi_{RF}(\mathbf{x})). \quad (30)$$

In practice, we use the usual instruction-tuning format in which  $(\mathbf{q}, \mathbf{y})$  are concatenated into a single text sequence with appropriate role markers, the RF tokens  $\phi_{RF}(\mathbf{x})$  are injected as a prefix, and gradients are applied only on the answer tokens  $\mathbf{y}$ . The key point is that *all* supervision is RF-grounded, by construction, every target token in  $\mathbf{y}$  must be consistent with the underlying RF scene,  $\mathbf{x}$ . This encourages the model to align RF patterns in the spectrogram with RF concepts in language compared to generic VLMs that have no RF prior, as we will demonstrate in Sec. IV.

## III. RF GROUNDING AND BENCHMARKING

With the modeling framework defined, a key requirement is a high-quality RF spectrogram–caption dataset. For each RF observation, we require a detailed and technically accurate natural-language description of the signal behavior in the time–frequency domain. RF spectrogram captioning requires domain expertise in modulation formats, multi-standard co-existence, scheduling, interference, and impairments. On the one hand, manual RF labeling is considered expensive and unreliable. On the other hand, existing VLMs are not RF-aware enough to generate trustworthy captions on their own. As a

result, generating high-quality RF–text pairs becomes technically demanding. Building such a dataset from real over-the-air measurements is also challenging. Capturing high-fidelity RF data requires specialized hardware, well-calibrated front-ends, and carefully planned measurement campaigns across different bands, locations, and times. Also, accurate ground truth is usually hidden inside base-station schedulers or proprietary devices and inaccessible by an external receiver. Finally, the typical RF environment is highly imbalanced, where common technologies and load conditions dominate, while rare but critical edge cases (e.g., extreme interference or unusual coexistence patterns) are barely observed. Hence, achieving both diversity and statistical coverage with purely real-world data require an industrial-scale, multi-operator effort that is beyond the scope of typical academic work.

For these reasons, we aimed for synthetic datasets generated by accurate standards-compliant software. The simulation gives us perfect access to all latent variables of interest, including exact modulation types, SNR values, bandwidth, start times, durations, resource block allocations and so on. We can systematically sweep across technologies, numerologies, channel bandwidths, traffic patterns, coexistence scenarios, and impairment levels to achieve a diversity and coverage that would be normally expensive to obtain from measurements. Synthetic data also enables precise, unambiguous captions that reflect the full underlying configuration, which is exactly the supervision needed to train an RFLM to reason about RF measurements.

### A. Wireless Technology Waveform Generation

We use MATLAB’s Wireless Waveform Generator family (5G Toolbox, LTE Toolbox, UMTS Toolbox, WLAN Toolbox, Satellite Communications Toolbox, Bluetooth Toolbox) as a unified tool to generate synthetic, realistic RF waveforms. Rather than describing each technology pipeline independently, we follow a common workflow that we design for six major wireless technologies, namely, 5G NR, LTE, UMTS, WLAN, DVB-S2, and Bluetooth.

- **Technology and configuration sampling:** We first select a target technology (e.g., 5G NR or WLAN) and create a base configuration object using the corresponding MATLAB API (e.g., `nrWaveformGenerator`). From this base, we define a bounded but rich parameter space for each technology (bandwidth, numerology or subcarrier spacing, modulation and coding scheme, frame structure, resource allocations, pilot and reference signals, etc.) and randomly sample a candidate configuration.
- **Realistic waveform generation:** The sampled configuration is passed to the toolbox waveform generator, which implements the relevant 3GPP/ETSI/IEEE physical-layer specifications. If the toolbox returns an error or detects a violation of standard constraints e.g., invalid physical resource block (PRB) or resource unit (RU) allocation, incompatible bandwidth and numerology, inconsistent pilot patterns, the configuration is rejected and a new sample is drawn. This rejection-sampling procedure ensures that all accepted waveforms are standards compliant.

- **Channel and impairment modeling:** For each waveform or scene, we optionally apply channel models and impairments (e.g., fading profiles, frequency-selective channels) and adjust noise levels to target specific SNR ranges. The exact channel and SNR parameters are recorded as part of the metadata.
- **Spectrogram construction:** The resulting complex baseband IQ waveform is converted into a time–frequency representation via an STFT. We apply magnitude or power compression (e.g., dB scaling) and map the spectrogram to a grayscale or pseudo-RGB image with fixed resolution, which will serve as input to the RF encoder.
- **Metadata logging:** For every accepted sample, we store (i) the waveform and the corresponding spectrogram image, (ii) the full configuration object returned by MATLAB (technology, numerology, bandwidth, frame and resource-grid settings, per-user allocations, PHY modes, etc.), (iii) any additional channel or noise parameters, and (iv) derived attributes used later by the captioner (e.g., link direction, number of users, modulation family, time/frequency occupancy and overlaps). These machine-readable metadata provide perfect ground truth for captioning, instruction synthesis, and benchmarking.

This common workflow is designed for each of the six considered technologies, with technology-specific APIs, parameter ranges, and validation checks. For each technology the MATLAB API used, the main configurable parameters, the randomization strategy, the validation logic, and the metadata fields stored are omitted due to page limit. Together, these six technology-specific generators give us a unified, standards-compliant synthetic datasets that covers a broad range of the wireless scenarios. Because every spectrogram is generated from a known configuration object and we keep that object verbatim, we obtain exact and noise-free labels for modulation type, bandwidth, numerology, scheduling, and link-level structure annotations. Examples of each wireless technology are provided in Fig. 2 for reference. These standardized waveforms and their metadata form the basis for the captioning and instruction-synthesis pipeline described next.

### B. Spectrogram Instruction Synthesis

The captioning stage produces, for each spectrogram, a structured record that combines machine-readable signal metadata (technology, modulation, bandwidth, time/frequency extents, SNR, overlaps, etc.) with a dense natural-language description of the scene. While these captions are technically accurate, they are (i) over-detailed, (ii) presented in a fixed order, and (iii) not formatted as instructions. Directly training on such monolithic captions makes optimization difficult and does not match the instruction-following setting we target for RF-GPT. To mitigate this, we (i) decompose caption information into several levels of difficulty and importance, and (ii) convert captions into diverse instruction–answer pairs using a text-only LLM. Specifically, we categorize caption information into five **information levels**:

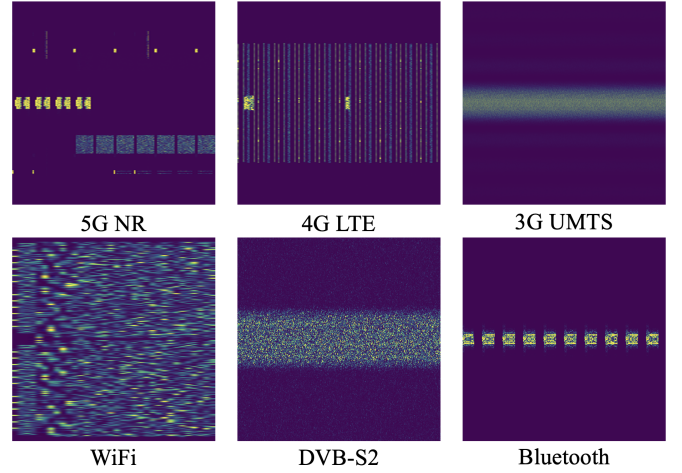


Fig. 2: Wireless technologies gallery: time-frequency spectrograms from six important RF signals including 5G NR, 4G LTE, 3G UMTS, WLAN, DVB-S2 and Bluetooth from (top left to bottom right).

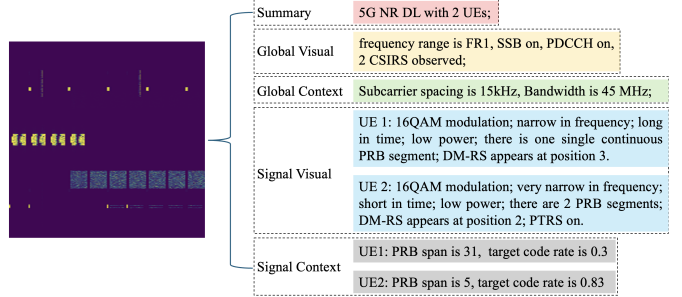


Fig. 3: Our fine-grained caption strategy for RF spectrograms. Metadata-derived information is grouped into five levels (summary, global visual, global context, signal visual, signal context), which are selectively combined when generating captions and instructions.

- **Summary:** high-level description of the RF recording (e.g., “a 5G NR downlink spectrogram containing several user data channels and synchronization signals”).
- **Global visual:** global visual patterns that can be directly captured in the spectrogram e.g., presence of synchronization signal blocks, channel state information reference signal (CSI-RS)/ sounding reference signal (SRS) bursts, overall occupancy and structure.
- **Global context:** spectrogram-level parameters that are not visually obvious but are known from metadata (e.g., channel bandwidth, subcarrier spacing, total time duration).
- **Signal visual:** per-signal visual attributes (relative SNR and time/frequency occupancy).
- **Signal context:** per-signal contextual parameters that are hard to infer visually, e.g., demodulation reference signal (DM-RS)/phase tracking reference signal (PTRS) settings for a given UE, detailed PDCCH/PUCCH structure.

Each instruction is constructed to present only a subset of these levels, so that the model focuses on a few related concepts per

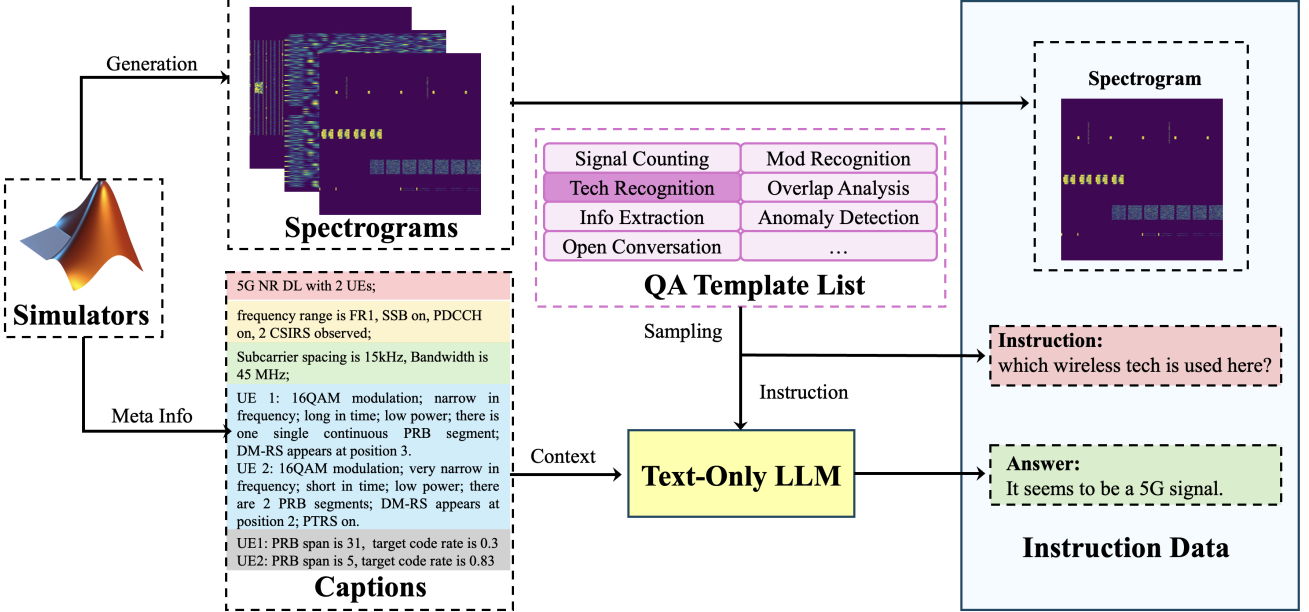


Fig. 4: Instruction synthesis pipeline. A deterministic captioner converts metadata into a dense caption, which is then fed to a text-only LLM to generate multiple RF-grounded instruction–answer pairs.

training example. In this work we mainly target summary and visual information (summary, global visual, signal visual) and leave fine-grained signal context, such as full DM-RS/PTRS or control resources set (CORESET) configurations, as future work. An example of a 5G NR spectrogram with its caption is illustrated in Fig. 3.

**Instruction synthesis pipeline.** Starting from the caption JSON/JSONL files, we build an instruction-tuning dataset via the following steps (see Fig. 4 for an overview):

- 1) **Load caption records:** We load the caption shards generated by captioning pipeline. Each record contains (i) structured signal metadata and (ii) one or more natural-language captions derived from that metadata.
- 2) **Sample a task template:** For each record, the instruction builder samples a task template from a predefined library. Templates cover tasks such as signal counting, modulation or technology recognition, information extraction (e.g., SCS or number of UEs), overlap analysis, consistency checks, and open-ended description.
- 3) **Assemble the prompt:** Given a selected template, we construct a prompt for a text-only LLM by combining a default *system prompt* that describes the role of the model (“You are an RF expert...”), a task-specific *user prompt* (e.g., “How many distinct signals are present?”), and a selected subset of caption fields provided as hidden/internal context (not shown to the end user). These fields are drawn from the information levels above. Optional global or signal-level context blocks are added depending on the template and difficulty, allowing us to control how much metadata the LLM can use when formulating the answer.
- 4) **Generate with a text-only LLM:** The assembled prompt is sent to a powerful text-only LLM, which produces a candidate response. The LLM is instructed

to follow specific output formats depending on the template, such as plain labels (for classification), JSON snippets (for structured extraction), or short paragraphs (for explanations and open-ended QA).

- 5) **Write instruction–answer pairs:** Successful pairs are recorded into dataset. Each entry contains the waveform identifier, the user-visible instruction, the target answer, the task type, and bookkeeping information (e.g., difficulty level and template ID).

This process converts heavy, deterministic captions into a large set of RF-grounded instruction–answer pairs that efficiently reflect how human experts query RF recordings. By controlling the task templates, information levels, and validation rules, we obtain a diverse and well-structured instruction dataset suitable for SFT of RF-GPT in an instruction-following setting. Beyond the scenarios around wireless technologies, to further enhance the diversity of modulation types, we also leverage TorchSig [33] to generate diverse wide-band modulation classes. The workflow of captioning and instruction generation is similar. We remove the details here to avoid duplication. The resulting instruction–answer pairs constitute our RF instruction-tuning dataset and also serve as the source for constructing the evaluation benchmarks in the following subsection.

### C. Benchmark Constructions

Following the construction of the instruction datasets, we perform RF-grounded instruction tuning to transform a general-purpose VLM into an RFLM. To systematically evaluate the RFLM’s RF understanding, we construct a comprehensive suite of benchmarks that tests the component recognition, quantity counting, and time/frequency relationship reasoning.

1) *Wide-Band Modulation Classification (WBMC)*: We extend our previous work on narrowband (single-signal) modulation classification with 57 modulation classes based on TorchSig [34] to a wideband setting with multiple, overlapping signals. In WBMC, each spectrogram contains 2–5 signals that may overlap in time and frequency. This benchmark evaluates the RFLM’s ability to identify the modulations present in a wideband RF scene. We define three sub-tasks of increasing difficulty:

- **Easy**: identify the set of modulation *families* present in the spectrogram.
- **Medium**: identify the exact modulation class of each signal from a given candidate list.
- **Hard**: identify the exact modulation class of each signal from the full list of modulation classes.

Let a spectrogram contain  $S$  signals with ground-truth modulation classes  $C = (c_1, \dots, c_S)$  according to their start time and let the model output  $M$  predicted classes  $C' = (\hat{c}_1, \dots, \hat{c}_{S'})$  using the same temporal ordering. We define the per-example classification score with strict time order and number matching as,

$$s^{\text{CLS}} = \begin{cases} \frac{1}{N} \sum_{i=1}^N \mathbb{1}\{\hat{c}_i = c_i\}, & \text{if } S = S', \\ 0, & \text{otherwise.} \end{cases} \quad (31)$$

In other words, if the predicted number of signals does not match the ground truth ( $S \neq S'$ ), the answer receives a zero score. WBMC performance is reported as the average  $s^{\text{CLS}}$  over the test set for each difficulty level. For each level, we generate 2000 visual question–answer (VQA) pairs from RF samples with the co-channel overlap probability set to zero, so that overlapping signals do not affect the modulation classification results severely<sup>1</sup>. Time/frequency overlap analysis is instead evaluated separately by the benchmark introduced below.

2) *Wide-Band Overlap Detection (WBOD)*: WBOD evaluates whether an RFLM can reason about how RF signals overlap in time and frequency. Each spectrogram contains multiple signals, and for each signal  $i$  we derive from the metadata:

$$T_i = [t_i^{\text{start}}, t_i^{\text{end}}], \quad F_i = [f_i^{\text{low}}, f_i^{\text{high}}], \quad (32)$$

where  $T_i$  is the time support interval and  $F_i$  is the frequency support interval. We define the pairwise overlap type for given two signals  $A$  and  $B$  as

$$\begin{aligned} o_t(A, B) &= \mathbb{1}(|T_A \cap T_B| > 0), \\ o_f(A, B) &= \mathbb{1}(|F_A \cap F_B| > 0), \end{aligned} \quad (33)$$

indicating whether they overlap in time and frequency, respectively. The pairwise overlap type  $L_{\text{type}}(A, B)$  is then

$$L_{\text{type}}(A, B) = \begin{cases} \text{neither,} & o_t = 0, o_f = 0, \\ \text{time-only,} & o_t = 1, o_f = 0, \\ \text{frequency-only,} & o_t = 0, o_f = 1, \\ \text{both,} & o_t = 1, o_f = 1. \end{cases} \quad (34)$$

<sup>1</sup>As noted in the TorchSig documentation, setting the co-channel overlap probability to zero does not completely eliminate overlapping signals.

**Easy (global overlap estimate):** The easy WBOD task asks for a *single* label describing the overall overlap situation in the spectrogram (“neither”, “time-only”, “frequency-only”, or “both”). We compute  $L_{\text{type}}(A, B)$  for all unordered pairs  $(A, B)$  and aggregate as follows:

- If any signals pair has  $L_{\text{type}}(A, B) = \text{both}$ , the global label is **both**.
- Else if there exists at least one pair with  $L_{\text{type}} = \text{time-only}$  and at least one pair with  $L_{\text{type}} = \text{frequency-only}$ , the global label is also **both**.
- Else if there is at least one pair with  $L_{\text{type}} = \text{time-only}$ , the global label is **time-only**.
- Else if there is at least one pair with  $L_{\text{type}} = \text{frequency-only}$ , the global label is **frequency-only**.
- Otherwise, the global label is **neither**.

The model is prompted with an instruction such as “Describe whether any signals overlap in time and/or frequency” and its answer is compared against this global label.

**Medium (pairwise overlap estimate):** The medium WBOD task focuses on specific signal pairs. The instruction identifies two signals (e.g., by index or description), and the model must output one of the four overlap types. Ground truth is simply  $L_{\text{type}}(A, B)$  as defined above. Accuracy is the fraction of correctly predicted types over all evaluated pairs.

**Hard (overlap strength estimate):** The hard WBOD task asks not only whether two signals overlap, but also how strongly they overlap along each axis. For a pair  $(A, B)$ , we define time- and frequency-overlap ratios

$$r_t(A, B) = \frac{|T_A \cap T_B|}{|T_A \cup T_B|}, \quad r_f(A, B) = \frac{|F_A \cap F_B|}{|F_A \cup F_B|}, \quad (35)$$

with  $r_t, r_f \in [0, 1]$ . We quantize each ratio  $r$  into one of four levels via

$$\ell(r) = \begin{cases} \text{none,} & r < 0.01, \\ \text{slightly,} & 0.01 \leq r < 0.3, \\ \text{considerably,} & 0.3 \leq r < 0.6, \\ \text{almost fully,} & r \geq 0.6. \end{cases} \quad (36)$$

The hard label for a pair is therefore the ordered pair  $(\ell(r_t(A, B)), \ell(r_f(A, B)))$  encoding the strength of overlap in time and frequency separately. The model is asked to describe the overlap strength (e.g., “time: slightly, frequency: almost fully”), hence, we parse its output and compute accuracy as the fraction of pairs for which both components match the ground-truth labels. In practice, WBOD-Easy asks about overlap in the entire scene, WBOD-Medium targets specific signal pairs, and WBOD-Hard quantizes the degree of overlap in time and frequency separately into four levels. To keep the task well-posed and avoid ambiguous references in crowded scenes, WBOD-Medium/Hard only consider **adjacent** signals in the time- or frequency-sorted order. This focuses evaluation on the most visually relevant local interactions (where overlap is actually likely) and avoids turning WBOD into a combinatorial “find any pair” search that would entangle it with the modulation-recognition task, i.e., WBMC. Similar to WBMC, there are 2000 VQAs for each level of difficulty based on RF

samples with co-channel overlapping probability 0.6 and SNR varying from 10-50 dB.

3) *Wireless Technology Recognition (WTR)*: For WTR, an RFLM is required to identify the wireless technology present in a spectrogram and, when applicable, the link direction (downlink vs. uplink). The label space consists of technology–direction pairs derived directly from the waveform generator configuration for technologies including NR, LTE, and WLAN. Performance is reported as standard top-1 classification accuracy over the test set. The test set contains 1000 samples for each of DVB-S2, Bluetooth, UMTS, and LTE, 1000 NR downlink and 1000 NR uplink signals, and 1000 WLAN-AX (11ax) and WLAN-BE (11be) signals.

4) *WLAN Number of Users Counting (WNUC)*: WNUC evaluates an RFLM’s ability to estimate the number of simultaneous users present in a wideband WLAN spectrogram. Each sample is labeled with the ground-truth user count  $U$ , denotes the number of distinct WLAN users that are active within the time–frequency window represented by the spectrogram. This can be obtained from the WLAN configuration metadata. Instead of predicting the exact number of users, we formulate an easier classification task by grouping user counts into fixed-size intervals. Hence, we define three difficulty levels:

- **Easy (15-user buckets)**: classification over coarse bins of size  $B = 15$ . The label is the bucket interval  $[s, e]$  where

$$s = \left\lfloor \frac{U-1}{B} \right\rfloor B + 1, \quad e = s + B - 1. \quad (37)$$

For example, with  $B = 15$  and  $U = 17$ , we obtain  $[s, e] = [16, 30]$ .

- **Medium (10-user buckets)**: identical to Easy but with  $B = 10$ . For instance, with  $B = 10$  and  $U = 17$ , we obtain  $[11, 20]$ .
- **Hard (numeric with rounding)**: the model outputs a single integer  $\hat{U}$ . If  $U < 10$ , the correct answer is the exact count. If  $U \geq 10$ , the correct answer is the nearest multiple of 10 (standard rounding):

$$\hat{U}^* = \begin{cases} U, & U < 10, \\ 10 \cdot \text{round}(U/10), & U \geq 10. \end{cases} \quad (38)$$

For easy and medium levels, we report bucket-level accuracy (predicted interval matches the true interval). For hard level, we report the fraction of examples where the predicted integer equals  $\hat{U}^*$ . Our benchmark test set consists of 1000 WLAN-AX samples and 1000 WLAN-BE samples.

5) *New Radio Information Extraction (NRIE)*: NRIE focuses on interpreting 5G NR spectrograms because (i) NR is a dominant cellular standard and (ii) its time–frequency structure encodes rich PHY-layer information. Each NRIE sample presents a single NR spectrogram (e.g., a 10 ms window) and asks the model to answer *one* question about a specific attribute. The evaluated attributes are:

- **Number of UEs**: estimate how many distinct UE transmissions are present. The response is a single integer, derived from the model’s text output.

- **Subcarrier spacing (SCS)**: classify the SCS in kHz from a discrete candidate set (dataset-specific). The response must be one of the listed numeric labels (e.g., “15”, “30”).
- **SSB pattern (DL only)**: identify the SSB pattern (e.g., A/B/C/...) for downlink spectrograms. If no SSB is present, the label is “N/A”.
- **CSI-RS count (DL only)**: count the number of distinct CSI-RS resources configured in downlink. The response is a single integer.
- **SRS count (UL only)**: count the number of distinct SRS resources in uplink, the response is a single integer.

NRIE therefore evaluates a model’s ability to extract key NR parameters from visual evidence alone, with some questions conditioned on link direction (DL/UL). For all NRIE tasks, we report exact-match accuracy between the parsed model output and the ground-truth label. Our test set for NRIE consists of 1000 DL samples and 1000 UL samples. More fine-grained NR features, such as PTRS and per-UE DMRS patterns or detailed PDCCH/PUCCH and CORESET configurations, will be considered in future work. It is worth noting that the hard-level benchmarks are designed to require a certain degree of reasoning capability, such that they can serve as meaningful indicators for future RFLMs.

## IV. EVALUATIONS

### A. Experimental Settings

We build RF-GPT on top of Qwen2.5-VL with 3B and 7B parameters, denoted as RF-GPT-3B and RF-GPT-7B, respectively, each of which is fine-tuned on the synthetic RF instruction dataset. As baselines, we evaluate the off-the-shelf Qwen2.5-VL-3B-Instruct, Qwen2.5-VL-7B-Instruct, and GPT-5 without any RF-specific fine-tuning. We fine-tune both models, RF-GPT-3B and RF-GPT-7B, with 3 epochs using AdamW [35] with learning rate  $2 \times 10^{-4}$ , global batch size 256, 5% warm-up and a cosine decay schedule. All models are trained with mixed precision (BF16) in PyTorch on 8 NVIDIA H200 GPUs with 140 GB video memory. For all experiments, complex baseband IQ sequences are converted into spectrograms using an STFT with a Blackman window (no centering, FFT shift along the frequency axis), FFT size 512, window length 512 samples, and hop size 512 samples. The magnitude spectrogram is converted to dB, clipped to a fixed dynamic range, and resized to  $512 \times 512$  pixels, the vision encoder processes non-overlapping  $14 \times 14$  patches, yielding 1369 RF tokens per spectrogram. All RF instructions are generated following the procedure explained in Sec. III with GPT-OSS-120B [36]. In total, our synthetic pipeline generates approximately 12,000 distinct RF scenes and 0.625 million RF-grounded instruction–answer pairs.

### B. General-Purpose VLMs Have No RF Priors

To further motivate RF-GPT framework and showcase its potential, we first study whether existing general-purpose VLMs possess any useful RF prior. First, we compare the response of RF-GPT-7B and its base model Qwen2.5-VL-7B-Instruct for a concrete 5G DL signal in Fig. 5. We can observe that the response of general-purpose VLM is shallow and does

not provides any meaningful information. On the other hand, RF-GPT provides a grounded and accurate answers including SSB patterns, existence of CSI-RS, number of UEs and their time/frequency occupancy.

Then, we evaluate Qwen2.5-VL-3B-Instruct, Qwen2.5-VL-7B-Instruct, and GPT-5 directly on our RF benchmarks, using carefully designed prompts that:

- explicitly state that the input image is an RF spectrogram,
- describe the axes as time (horizontal) and frequency (vertical),
- and ask for concrete, machine-parsable answers (modulation labels, overlap categories, counts, etc.).

Despite the well-designed prompt, the scores of these models are close to random guessing, where models either limit their output to a few frequent labels, or distribute their predictions almost uniformly across the candidate options, indicating a lack of meaningful RF priors. On WBMC (Fig. 6), general-purpose models’ accuracies are within a few percent of random guessing, and they almost never predict the correct number of signals (below 5%). However, RF-GPT models scored exceptional accuracy performance exceeding 97%. On WBOD (Fig. 7), the performance of general-purpose ones when tested on easy, medium, and hard overlap tasks is similarly low (typically in the single-digit to low-teens percentage range), again emphasizing chance-level prediction. On WTR (Fig. 8), the tested models exhibit biased predictions, frequently over-predicting LTE downlink and underperforming on most other technologies and link directions. For WNUC and NRIE (Fig. 10 and Fig. 11), performance remains low. In many cases, predictions appear to rely on simple heuristics, or the models produce free-form outputs that cannot be reliably parsed and are therefore marked as incorrect. These results confirm that **current general-purpose VLMs have no RF prior**, any non-zero scores are stemmed from random guessing and not from real RF understanding. This motivates RF grounding and specialized instruction tuning, as done in RF-GPT.

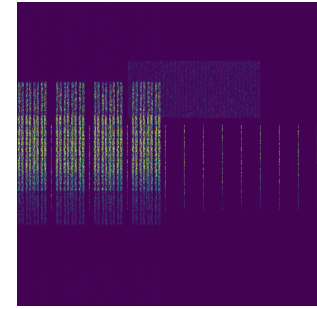
### C. Benchmark Results: RF-GPT vs. General-purpose Models

Here, We present the performance of RF-GPT on the proposed benchmarks and compare it against general-purpose VLMs. Across all tasks, RF-GPT dramatically outperforms the baseline models, validating the effectiveness of spectrogram-based RF grounding. This was clearly demonstrated through the scores of general-purpose VLMs, where their predictions behave like different forms of randomness, depending on the prompt and model. Therefore, the scores of general-purpose VLMs serve as a comparison reference only.

**WBMC:** Fig. 6 presents the WBMC results. General-purpose VLMs achieve at most 7% accuracy on the easy task and close to 0% on the hard task, with an average score below 2%. These extreme low scores are due to our strict time-order awareness and number matching criteria. In fact, most of general-purpose VLMs fail to predict the number of signals presented in the spectrogram. In contrast, RF-GPT-3B reaches 80.0% / 71.4% / 43.7% accuracy on Easy / Medium / Hard, and RF-GPT-7B further improves the accuracy performance to 82.4% / 74.2% / 47.8%, with respect to the same levels. The

### An Example of 5G NR Downlink Spectrogram with One UE

**User:** Describe what do you observe in this RF scene.



**Qwen-2.5-VL-7B-Instruct:** This spectrogram displays a variety of radio-frequency (RF) signals. In the central region, there are several prominent vertical lines, suggesting strong, narrowband transmissions that could be from specific transmitters such as amateur radio stations, radar systems, or other point-to-point communication devices. To the right, there are fainter, more dispersed lines, which might indicate lower power transmissions or background noise. The overall pattern suggests a mix of active and passive RF activity within the observed frequency range.

**RF-GPT-7B:** The spectrogram shows a single-UE **5G-NR** downlink capture in the **FR2** band. A SSB is present, following the **Case D** transmission pattern, and the PDCCH is also active. **No CSI-RS** traces are visible, confirming that CSI-RS transmission is disabled for this capture. The data payload occupies one continuous block of PRBs. The occupied bandwidth is moderate. In the time dimension the burst is **short**, lasting only a few symbols before the signal fades. The overall power level of the burst is **low**, giving the spectrogram a faint intensity compared with typical high-power carriers.

Fig. 5: Comparison between general-purpose VLM and RF-GPT on a 5G DL spectrogram with only one UE. General-purpose VLM such as Qwen2.5-VL-7B has no RF prior and fails to extract any useful information from the spectrogram.

average score increases largely after RF-grounded finetuning of both 3B and 7B models. Importantly, RF-GPT correctly identifies the number of signals in around 98% of the cases, while general VLMs almost fail all the cases. These results indicate that RF-GPT can both estimate the number of active signals and correctly identify their modulation types in complex wideband input.

**WBOD:** WBOD results are shown in Fig. 7. General-purpose VLMs perform marginally above chance. Their easy-level accuracies range from approximately 23–25%, medium-level accuracies remain around 30%, and hard-level time–frequency overlap classification drops to 5–12%, resulting in overall average scores of roughly 11–16%. These

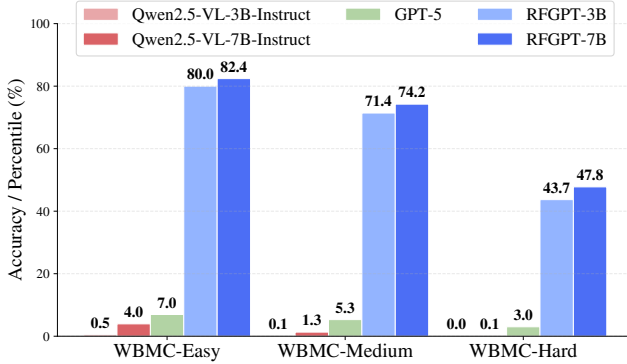


Fig. 6: Benchmark scores on the wide-band modulation classification (WBMC) tasks. RF-GPT can classify modulation presented in a spectrogram in coarse modulation family while general-purpose VLMs have almost no knowledge on RF modulations. In fact, most of the time these models fail to identify the number of presented RF signals.

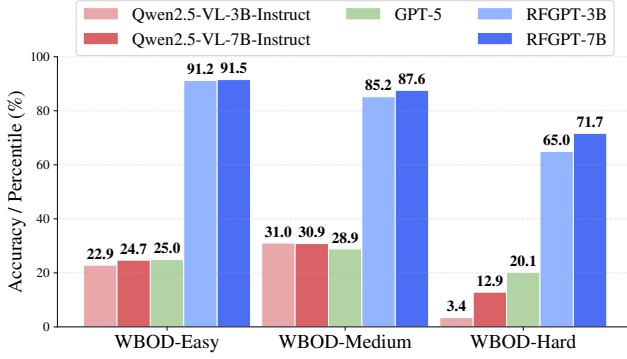


Fig. 7: Benchmark scores on the wide-band overlap detection (WBOD) tasks. RF-GPT can perform overall and per-pair overlap detection in both time and frequency domains, whereas general-purpose VLMs behave close to random.

numbers are partly influenced by a biased prediction pattern in which the models frequently select the “none” label, even though only a small fraction of signal pairs exhibit no overlap in either time or frequency. In contrast, RF-GPT-3B achieves 91.2% (Easy), 85.2% (Medium), and about 65.0% accuracy on the hard joint time–frequency overlap task. RF-GPT-7B further improves the hard-task accuracy to 71.7%, with similar or slightly better performance on the easy and medium tasks. These results indicate that RF-GPT can reason coherently about whether signals overlap in time and frequency and to what extent, whereas generic VLMs produce essentially random overlap labels.

**WTR:** Fig. 8 summarizes WTR performance. Qwen2.5-VL series achieve a joint technology+link accuracy of only 5.01% (3B) and 4.98% (7B), with highly inconsistent behavior across technologies. For example, Qwen2.5-VL-3B-Instruct predicts LTE reasonably often but almost never identifies NR, UMTS, WLAN, or DVB-S2 correctly, and its link-direction predictions are heavily biased (e.g., always “DL”). GPT-5 does not

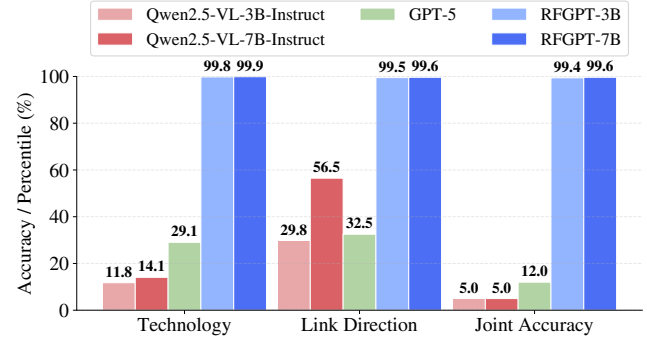


Fig. 8: Benchmark results for wireless technology recognition (WTR) benchmark. RF-GPT nearly perfectly identifies wireless technologies and link directions, while general-purpose VLMs collapse on most classes.

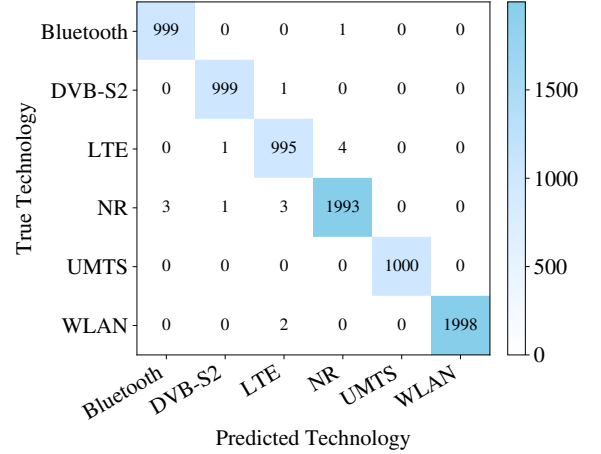


Fig. 9: Confusion matrix of WTR task. RF-GPT is capable of identifying different technologies with almost perfect accuracy.

produce any consistent correct predictions under our parsers. In contrast, RF-GPT-3B achieves 99.42% joint accuracy, with almost perfect per-technology and per-link scores ( $\geq 99.5\%$  on most classes). RF-GPT-7B further improves to 99.64% joint accuracy and close to 100% on most individual technologies and link directions. This shows that RF-GPT has learned a highly reliable RF taxonomy across heterogeneous standards.

**WNUC:** WNUC results are presented in Fig. 10. General-purpose VLMs achieve average accuracies of 23.97% (3B) and 22.83% (7B) across all difficulty levels and both WLAN standards (11ax/11be). They struggle particularly on the hard (numeric) task, where accuracies are around 13–14%. After RF grounding, the same backbones achieve much higher scores, where the 3B model attains an average of 65.43%, and the 7B model reaches 70.17%. In particular, both model variants exhibit consistent higher performance in the 802.11be standard compared to 11ax. For RF-GPT-3B, we observe absolute accuracy gains of 13.7%, 6.6%, and 6.1% for the easy, medium, and hard difficulty levels, respectively. Similarly, for the larger RF-GPT-7B model, the gains are 12.2%,

6.6%, and 4.2%, respectively. This performance difference is stemmed from the different resource mapping strategies used during data generation. While 11be samples typically assign a single user per Resource Unit (RU), 11ax samples frequently involve multiple users sharing a single RU through MU-MIMO. The latter creates significant visual overlap in the time-frequency plane, masking the individual user signatures and making the counting task more challenging for a vision-based backbone compared to the spatially distinct OFDMA patterns in 11be. This demonstrates that RF-GPT can infer approximate user counts directly from OFDMA/MU-MIMO structures in WLAN spectrograms.

**NRIE:** NRIE results are shown in Fig. 11. General-purpose VLMs perform poorly on NR-specific attributes, with average accuracies around 20% and substantial variation across tasks (e.g., slightly better on UE count, but weak on SSB pattern and SCS). After RF grounding, RF-GPT-3B reaches an average accuracy of 72%, with near-perfect SCS and SSB pattern recognition and moderate performance on UE number estimation, CSI-RS, and SRS resources. RF-GPT-7B achieves similar or improved performance on most tasks (notably higher SRS and UE estimation), confirming that larger models can extract richer NR structure from spectrograms. Overall, NRIE shows that RF-GPT is not limited to generic modulation or technology recognition, but it can also recover protocol-specific parameters that are crucial for 5G NR analysis.

Taken together, these results show that RF-GPT consistently turns general-purpose VLMs, which have no RF prior, into strong RF foundation models that perform well across a diverse suite of benchmarks, including modulation classification, overlap analysis, technology recognition, number of users estimation, and NR-specific attribute extraction.

#### D. Ablation Studies

We perform ablation studies on different configurations. We select one benchmark that we believe to be the most sensitive to a given configuration and apply it to data samples related to this benchmark only instead of the whole dataset to avoid extra data processing.

**Robustness against impairments.** We start by evaluating the robustness of RF-GPT to common RF impairments. For impairment-sweep experiments, we vary one impairment family at a time, including IQ (IQ) imbalance, power amplifier (PA) nonlinearity, carrier frequency offset (CFO), or time-varying multipath (TDL), while reusing a common clean waveform as a base. We introduce a normalized impairment level  $\lambda \in \{0.2, 0.4, 0.6, 0.8, 1.0\}$ , with  $\lambda = 0$  corresponding to the clean baseline. During training, we include **only spectrograms with relatively mild impairments** ( $\lambda \leq 0.3$ ), so that robustness to larger distortions must arise from generalization rather than direct exposure during training. For IQ imbalance, the gain mismatch between I and Q branches increases from 0 to 8 dB and the phase mismatch from  $0^\circ$  to  $15^\circ$  across the sweep. For PA nonlinearity, we gradually move from a relatively linear amplifier with a high saturation level and smooth Rapp characteristic to a stronger, more abrupt saturation with lower effective backoff. CFO is swept

from 0 to 1200 Hz, and the TDL channel evolves from a flat channel to one with delay spreads up to  $500 \mu\text{s}$  and maximum Doppler shifts up to 200 Hz, with the TDL profile randomly chosen from TDL-C and TDL-D in the MATLAB API. This setup enables a controlled robustness analysis in which the impairment strength changes while the underlying waveform content remains fixed.

Fig. 12 reports NRIE performance of RF-GPT-7B under increasing impairment severity for CFO, TDL, PA, and IQ imbalance. Starting from a clean score of 76.31%, CFO and PA sweeps cause only minor degradation and the curves remain nearly flat, while TDL introduces a moderate drop. In contrast, IQ imbalance produces the largest and nearly monotonic performance decline, from 75.29% at the lowest nonzero level to 70.21% at the highest level (about 6.1 percentage points below clean). The observed ranking aligns with how each impairment alters spectrogram structure, where the CFO primarily shifts energy along the frequency axis while preserving local time-frequency patterns, moderate PA nonlinearity mainly compresses amplitudes and generates in-band distortion without radically changing the layout of NR structures, TDL spreads and fades components but often keeps coarse OFDM structure visible, IQ imbalance, however, introduces strong image-frequency components and cross-leakage, creating mirror-like or duplicated patterns that directly interfere with counting and structural cues used by NRIE (e.g., UE-related regions and reference-signal layouts), making it the most destructive of the considered impairments.

**Comparison with CNN/Transformer baselines.** To compare RF-GPT with strong non-LLM baselines, we implement spectrogram-based CNN and Transformer models for the NRIE benchmark. Each model takes the NR spectrogram as input, passes it through a shared backbone (e.g., EfficientNet [37] or ViT [24]), and applies global average pooling to obtain a feature vector. On top of this backbone, we attach separate task-specific heads for each NRIE attribute, reflecting the heterogeneous nature of the benchmark. The SCS and SSB heads are implemented as linear layers with softmax outputs over their respective label sets, whereas the counting heads are implemented as small classifiers over the admissible count range for number of UEs, CSI-RS and SRS, with the predicted integer given by the arg max of the logits. The overall NRIE loss is an equally weighted sum of the per-head cross-entropy terms. However, these task-specific customizations underscore the narrow generalization of conventional deep neural networks compared to a unified instruction-following RFLM.

Fig. 13 compares NRIE performance across training progress for RF-GPT and CNN/Transformer baselines including EfficientNet and ViT-B, ViT-H. RF-GPT-7B consistently achieves the best score, improving from 69.99% (epoch 1) to 76.96% (epoch 3). RF-GPT-3B also improves steadily, from 67.17% to 71.83% by epoch 3, which is already close to ViT-B at epoch 30 (72.34%) and slightly higher than EfficientNet at epoch 30 (70.85%). Among the non-LLM baselines, ViT-H is strongest, increasing from 65.21% to 76.39% by epoch 30, while ViT-B and EfficientNet reach 72.34% and 70.85%, respectively. Overall, RF-GPT-7B still outperforms the strongest ViT-H baseline slightly while using only 3

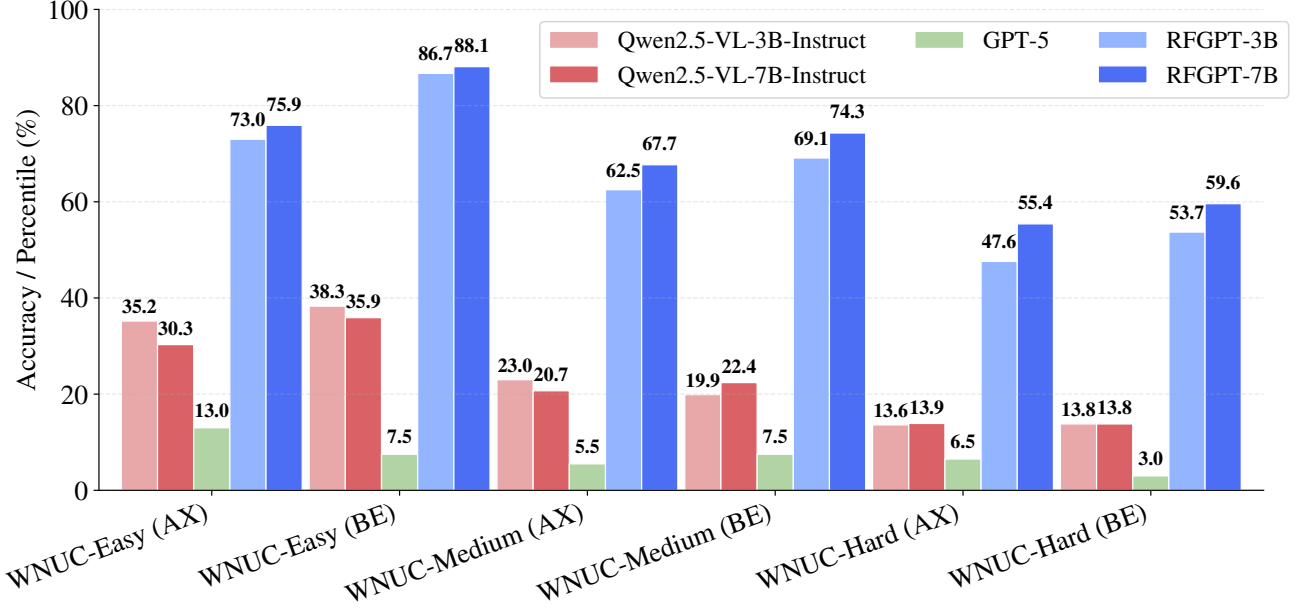


Fig. 10: Benchmark scores on the WLAN number of users counting (WNUC) tasks for 802.11ax and 802.11be. RF-GPT with different model sizes is capable of estimating the number of UEs directly from spectrograms.

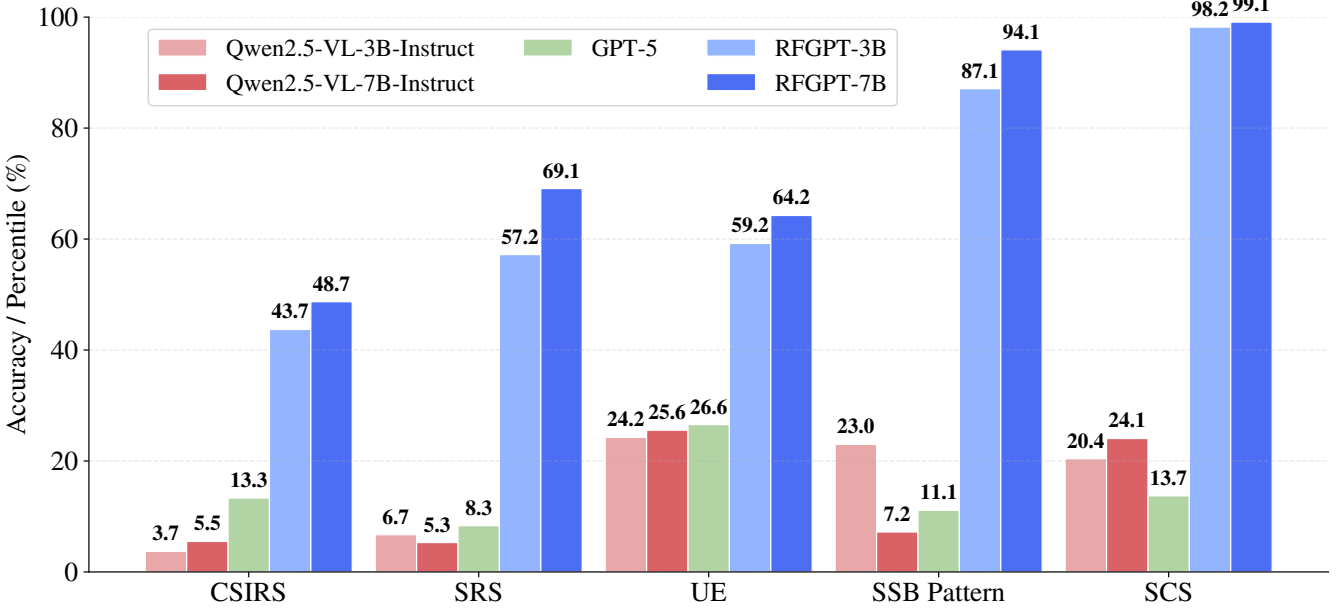


Fig. 11: Benchmark results for the New Radio information extraction (NRIE) benchmark. RF-GPT is capable of accurately extracting the SCS in kHz, identifying SSB pattern and estimating the number of UEs, CSI-RS and SRS.

epochs instead of 30, indicating better data efficiency and stronger instruction-conditioned RF reasoning. This behavior is related to the NRIE task structure, where jointly inferring heterogeneous attributes benefits from a unified language-conditioned model more than from fixed closed-set multi-head classifiers. The sharp improvement of RF-GPT-7B during training suggests that RF instruction tuning rapidly captures task-specific priors, whereas baseline models improve more

slowly even with extended training. In contrast to multi-head CNN or Transformer classifiers that require separate architectures and supervision for each NRIE task, RF-GPT relies on a unified model trained with a single token-level cross-entropy objective. Different NR attributes are handled naturally through language instructions, without modifying the architecture. This unified RF-language interface simplifies the overall design while producing structured, human-readable

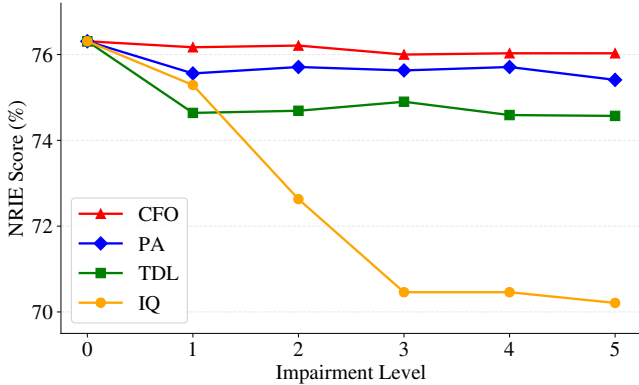


Fig. 12: NRIE ablation vs. impairment level of IQ imbalance (IQ), power amplifier nonlinearity (PA), time delay channel (TDL) and carrier frequency offset (CFO). RF-GPT maintains high accuracy except for IQ due to its destructive introduction of cross-leakage, mirror-like creation or duplicated patterns.

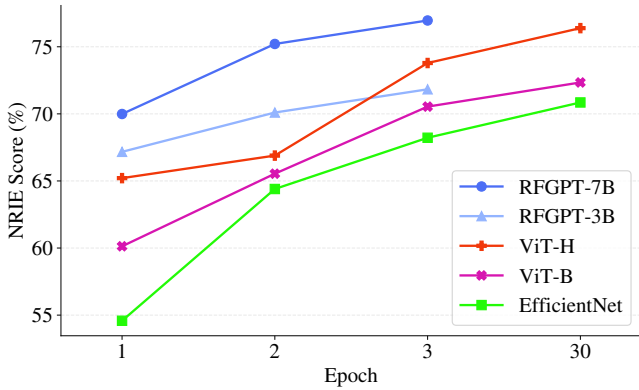


Fig. 13: NRIE ablation comparing RF-GPT and Transformer/CNN baselines across epochs; RF-GPT-7B consistently leads, and even after 30 epochs the best CNN/Transfomer baseline remains below RF-GPT, highlighting the advantage of RF-grounded finetuning.

outputs (e.g., explanations or JSON summaries) rather than only numeric predictions, making the system easier to interpret and integrate with higher-level LLM agents.

**Image resolution** We end the ablation study by analyzing the impact of input image resolution on WBMC. We evaluate **RF-GPT-7B** at 224, 384, and 512, as shown in Fig. 14. The performance improves consistently as resolution increases, where WBMC-Easy rises from 72.94%  $\rightarrow$  78.72%  $\rightarrow$  82.41%, WBMC-Medium from 64.52%  $\rightarrow$  71.26%  $\rightarrow$  74.24%, and WBMC-Hard from 39.64%  $\rightarrow$  43.76%  $\rightarrow$  47.94%. From 224 to 512, the absolute gains are +9.47 (Easy), +9.72 (Medium), and +8.30 (Hard) points. These results indicate that higher-resolution spectrograms preserve more discriminative time-frequency details and benefit both coarse and fine-grained modulation recognition. However, increasing image resolution also increases RF token count, leading to

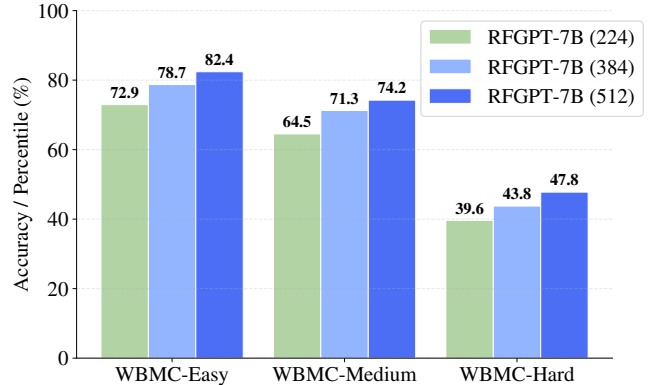


Fig. 14: WBMC ablation of RF-GPT-7B under different image resolutions. Larger image resolution leads to better accuracy thanks to finer RF tokens.

higher memory/computation cost and longer inference latency.

## V. CONCLUSION

In this paper, we introduce the concept of RFLM and present RF-GPT as its first realization. RF-GPT integrates RF spectrograms into a multimodal LLM, enabling a unified interface between RF signals and natural language. Through adopting realistic synthetic waveform generation, deterministic spectrogram captioning, and LLM-based instruction synthesis, we constructed a large RF instruction-tuning dataset spanning multiple technologies and tasks. On our comprehensive benchmarks, RF-GPT substantially outperformed general-purpose VLMs with no RF priors, and showed competitive performance with strong CNN and Transformer baselines, while additionally offering natural-language answers, structured outputs, and explanations from a single model. Our current RF grounding is mainly synthetic and limited to single-input spectrograms, motivating future work on real over-the-air data, multi-antenna and ISAC settings, and finer NR control-channel features. We also aim to integrate RF-GPT into spectrum-monitoring and AI-native network management prototypes, moving RFLMs from synthetic proof-of-concept toward practical RF intelligence engines for next-generation wireless networks.

## REFERENCES

- [1] A. Hurst, A. Lerer, A. P. Goucher, A. Perelman, A. Ramesh, A. Clark, A. Ostrow, A. Welihinda, A. Hayes, A. Radford *et al.*, “Gpt-4o system card,” *arXiv preprint arXiv:2410.21276*, 2024.
- [2] G. Comanici *et al.*, “Gemini 2.5: Pushing the frontier with advanced reasoning, multimodality, long context, and next-generation agentic capabilities,” *arXiv preprint arXiv:2507.06261*, 2025.
- [3] H. Liu *et al.*, “Visual instruction tuning,” *Advances in Neural Information Processing Systems*, vol. 36, pp. 34 892–34 916, 2023.
- [4] S. Bai *et al.*, “Qwen2.5-VL Technical Report,” *arXiv preprint arXiv:2502.13923*, 2025.
- [5] J. Zhu *et al.*, “InternVL3: Exploring Advanced Training and Test-Time Recipes for Open-Source Multimodal Models,” *arXiv preprint arXiv:2504.10479*, 2025.
- [6] A. Radford, J. W. Kim, T. Xu, G. Brockman, C. McLeavey, and I. Sutskever, “Robust speech recognition via large-scale weak supervision,” in *International conference on machine learning*. PMLR, 2023, pp. 28 492–28 518.

[7] Y. Chu, J. Xu, Q. Yang, H. Wei, X. Wei, Z. Guo, Y. Leng, Y. Lv, J. He, J. Lin *et al.*, “Owen2-audio technical report,” *arXiv preprint arXiv:2407.10759*, 2024.

[8] B. Zhang, C. Guo, G. Yang, H. Yu, H. Zhang, H. Lei, J. Mai, J. Yan, K. Yang, M. Yang *et al.*, “Minimax-speech: Intrinsic zero-shot text-to-speech with a learnable speaker encoder,” *arXiv preprint arXiv:2505.07916*, 2025.

[9] X. Tian, Q. Zheng, B. Li, D. Qiao, K. Yu, Z. Wei, B. Li, H. Jiang, X. Li, Y. Lin, and G. Gui, “A survey on deep learning enabled automatic modulation classification methods: Data representations, model structures, and regularization techniques,” *Signal Processing*, vol. 242, p. 110444, 2026.

[10] M. Cheraghinia, E. De Poorter, J. Fontaine, M. Debbah, and A. Shahid, “A foundation model for wireless technology recognition and localization tasks,” *IEEE Open Journal of the Communications Society*, vol. 6, pp. 9879–9896, 2025.

[11] S. Alikhani, G. Charan, and A. Alkhateeb, “Large wireless model (lwm): A foundation model for wireless channels,” *arXiv preprint arXiv:2411.08872*, 2024.

[12] T. Yang, P. Zhang, M. Zheng, Y. Shi, L. Jing, J. Huang, and N. Li, “Wirelessgpt: A generative pre-trained multi-task learning framework for wireless communication,” *IEEE Network*, 2025.

[13] J. Hoffmann, S. Borgeaud, A. Mensch, E. Buchatskaya, T. Cai, E. Rutherford, D. de Las Casas, L. A. Hendricks, J. Welbl, A. Clark *et al.*, “Training compute-optimal large language models,” in *Proceedings of the 36th International Conference on Neural Information Processing Systems*, 2022, pp. 30016–30030.

[14] A. Shahid *et al.*, “Large-scale AI in telecom: Charting the roadmap for innovation, scalability, and enhanced digital experiences,” *arXiv preprint arXiv:2503.04184*, 2025.

[15] Y. Zhao *et al.*, “A Comprehensive Survey of 6G Wireless Communications,” *arXiv preprint arXiv:2101.03889*, 2020.

[16] M. Giordani *et al.*, “6G: The Intelligent Network of Everything – A Comprehensive Vision and Tutorial,” *arXiv preprint arXiv:2407.09398*, 2024.

[17] L. Liang *et al.*, “Large Language Models for Wireless Communications: From Adaptation to Autonomy,” *arXiv preprint arXiv:2507.21524*, 2025.

[18] F. Zhu *et al.*, “Wireless large ai model: Shaping the ai-native future of 6g and beyond,” *arXiv preprint arXiv:2504.14653*, 2025.

[19] J. Shao *et al.*, “WirelessLLM: Empowering Large Language Models Towards Wireless Intelligence,” *arXiv preprint arXiv:2405.17053*, 2024.

[20] L. Baria, Q. Zhao, H. Zou, Y. Tian, F. Bader, and M. Debbah, “Large Generative AI Models for Telecom: The Next Big Thing?” *IEEE Communications Magazine*, vol. 62, no. 11, pp. 84–90, 2024.

[21] H. Zhou *et al.*, “Large Language Model (LLM) for Telecommunications: A Comprehensive Survey on Principles, Key Techniques, and Opportunities,” *IEEE Communications Surveys & Tutorials*, vol. 27, no. 3, pp. 1955–2005, 2025.

[22] H. Zou, Q. Zhao, Y. Tian, L. Baria, F. Bader, T. Lestable, and M. Debbah, “TelecomGPT: A Framework to Build Telecom-Specific Large Language Models,” *IEEE Transactions on Machine Learning in Communications and Networking*, vol. 3, pp. 948–975, 2025.

[23] A. Vaswani, N. Shazeer, N. Parmar, J. Uszkoreit, L. Jones, A. N. Gomez, Ł. Kaiser, and I. Polosukhin, “Attention is all you need,” in *Advances in Neural Information Processing Systems (NeurIPS)*, vol. 30, 2017.

[24] A. Dosovitskiy, L. Beyer, A. Kolesnikov, D. Weissenborn, X. Zhai, T. Unterthiner, M. Dehghani, M. Minderer, G. Heigold, S. Gelly *et al.*, “An image is worth 16x16 words: Transformers for image recognition at scale,” in *International Conference on Learning Representations (ICLR)*, 2021.

[25] H. Touvron, M. Cord, M. Douze, F. Massa, G. Synnaeve, and H. Jégou, “Training data-efficient image transformers & distillation through attention,” in *International Conference on Machine Learning (ICML)*. PMLR, 2021, pp. 10347–10357.

[26] P. Flandrin, *Time-Frequency/Time-Scale Analysis*. Academic Press, 1999.

[27] K. Jaganathan, Y. C. Eldar, and B. Hassibi, “Sftf phase retrieval: Uniqueness guarantees and recovery algorithms,” *IEEE Journal of selected topics in signal processing*, vol. 10, no. 4, pp. 770–781, 2016.

[28] E. J. Candes, T. Strohmer, and V. Voroninski, “Phaselift: Exact and stable signal recovery from magnitude measurements via convex programming,” *Communications on Pure and Applied Mathematics*, vol. 66, no. 8, pp. 1241–1274, 2013.

[29] J. Su, M. Ahmed, Y. Lu, S. Pan, W. Bo, and Y. Liu, “Roformer: Enhanced transformer with rotary position embedding,” *Neurocomputing*, vol. 568, p. 127063, 2024.

[30] B. Zhang and R. Sennrich, “Root mean square layer normalization,” in *Advances in Neural Information Processing Systems (NeurIPS)*, vol. 32, 2019.

[31] J. Ainslie, J. Lee-Thorp, M. de Jong, Y. Zemlyanskiy, W. Fedus, P. Sumers, G. Desjardins, A. Siddhant, Y. Ruiz, D. Luan *et al.*, “GQA: Training generalized multi-query transformer models from multi-head checkpoints,” *arXiv preprint arXiv:2305.13245*, 2023.

[32] N. Shazeer, “Glu variants improve transformer,” *arXiv preprint arXiv:2002.05202*, 2020.

[33] L. Boegner *et al.*, “Large scale radio frequency signal classification,” *arXiv preprint arXiv:2207.09918*, 2022.

[34] H. Zou, B. Wang, Y. Tian, L. Baria, C. Huang, S. Lasaluce, and M. Debbah, “Seeing radio: From zero rf priors to explainable modulation recognition with vision language models,” *arXiv preprint arXiv:2601.13157*, 2026.

[35] D. P. Kingma and J. Ba, “Adam: A method for stochastic optimization,” in *International Conference on Learning Representations (ICLR)*, 2015.

[36] S. Agarwal, L. Ahmad, J. Ai, S. Altman, A. Applebaum, E. Arbus, R. K. Arora, Y. Bai, B. Baker, H. Bao *et al.*, “gpt-oss-120b & gpt-oss-20b model card,” *arXiv preprint arXiv:2508.10925*, 2025.

[37] M. Tan and Q. V. Le, “Efficientnet: Rethinking model scaling for convolutional neural networks,” in *Proceedings of the 36th International Conference on Machine Learning*, ser. ICML. PMLR, 2019, pp. 6105–6114.